ACS OMEGA

Open Access

http://pubs.acs.org/journal/acsodf

Article

Nonenzymatic Potentiometric Detection of Ascorbic Acid with Porphyrin/ZnO-Functionalized Laser-Induced Graphene as an Electrode of EGFET Sensors

Kishore Pushparaj, Alexandro Catini, Rosamaria Capuano, Valerio Allegra, Gabriele Magna, Gianni Antonelli, Eugenio Martinelli, Antonio Agresti, Sara Pescetelli, Yuvaraj Sivalingam, Roberto Paolesse, and Corrado Di Natale*

Cite This: *ACS Omega* 2024, 9, 10650−10659

Read Online

ACCESS | Metrics & More | Article Recommendations

ABSTRACT: Laser-induced graphene (LIG) has emerged as a highly versatile material with significant potential in the development of electrochemical sensors. In this paper, we investigate the use of LIG and LIG functionalized with ZnO and porphyrins-ZnO as the gate electrodes of the extended gate field effect transistors (EGFETs). The resultant sensors exhibit remarkable sensitivity and selectivity, particularly toward ascorbic acid. The intrinsic sensitivity of LIG undergoes a notable enhancement through the incorporation of hybrid organic−inorganic materials. Among the variations tested, the LIG electrode coated with zinc tetraphenylporphyrin-capped ZnO nanoparticles demonstrates superior performance, reaching a limit of detection of approximately 3 nM. Furthermore, the signal ratio for 5 μM ascorbic acid relative to the same concentration of dopamine exceeds 250. The practical applicability of these sensors is demonstrated through the detection of ascorbic acid in real-world samples, specifically in a commercially available food supplement containing L-arginine. Notably, formulations with added vitamin C exhibit signals at least 25 times larger than those without, underscoring the sensors' capability to discern and quantify the presence of ascorbic acid in complex matrices. This research not only highlights the enhanced performance of LIG-based sensors through functionalization but also underscores their potential for practical applications in the analysis of vitamin-rich supplements.

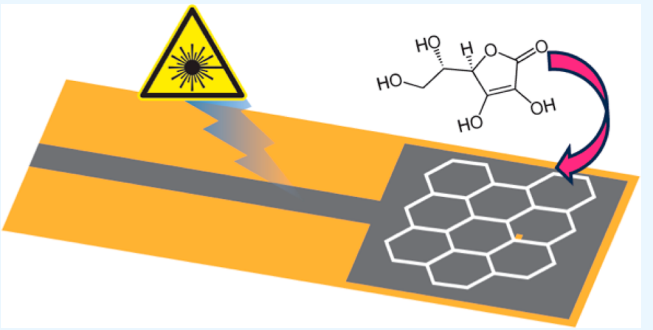

INTRODUCTION

L-Ascorbic acid, widely known as vitamin C, is a naturally occurring water-soluble antioxidant renowned for its protective properties against diseases induced by free radicals.[1] While plants and most animals can synthesize ascorbic acid, humans and other primates lack this capability and must obtain it through their diet. Due to its beneficial effects, ascorbic acid is an almost ubiquitous additive in various products, including pharmaceuticals, food, and beverages. Thus, the increasing significance of ascorbic acid in both medical and technological realms necessitates the development of dedicated analytical methods and sensors.[2,3]

The electron-donor characteristics of ascorbic acid facilitate its detection with amperometric sensors at an appropriate oxidation potential.[4] Alternatively, biosensors based on the ascorbate oxidase enzyme on metal oxides also make potentiometric detection possible.[5] In recent years, there has been a growing interest in the development of nonenzymatic sensors to improve robustness, stability, and cost with respect to conventional biosensors. For instance, the detection of glucose with inorganic nanostructured materials has shown comparable properties with respect to enzymatic sensors.[6−9]

This paper introduces a potentiometric nonenzymatic method for the detection of ascorbic acid employing an extended gate field effect transistor (EGFET) with the gate electrode fabricated from laser-induced graphene (LIG) on polyimide.

LIG is a simple and convenient method to produce patterned graphene from ordinary polymers.[10] Laser exposure induces localized temperatures above 2000 K, leading to the breakage of C−N, C−O, and C═O bonds and resulting in the formation of a porous 3D graphene structure with a high density of surface defects and pores, making it ideal for sensing

Received: November 16, 2023
Revised: January 30, 2024
Accepted: February 1, 2024
Published: February 22, 2024

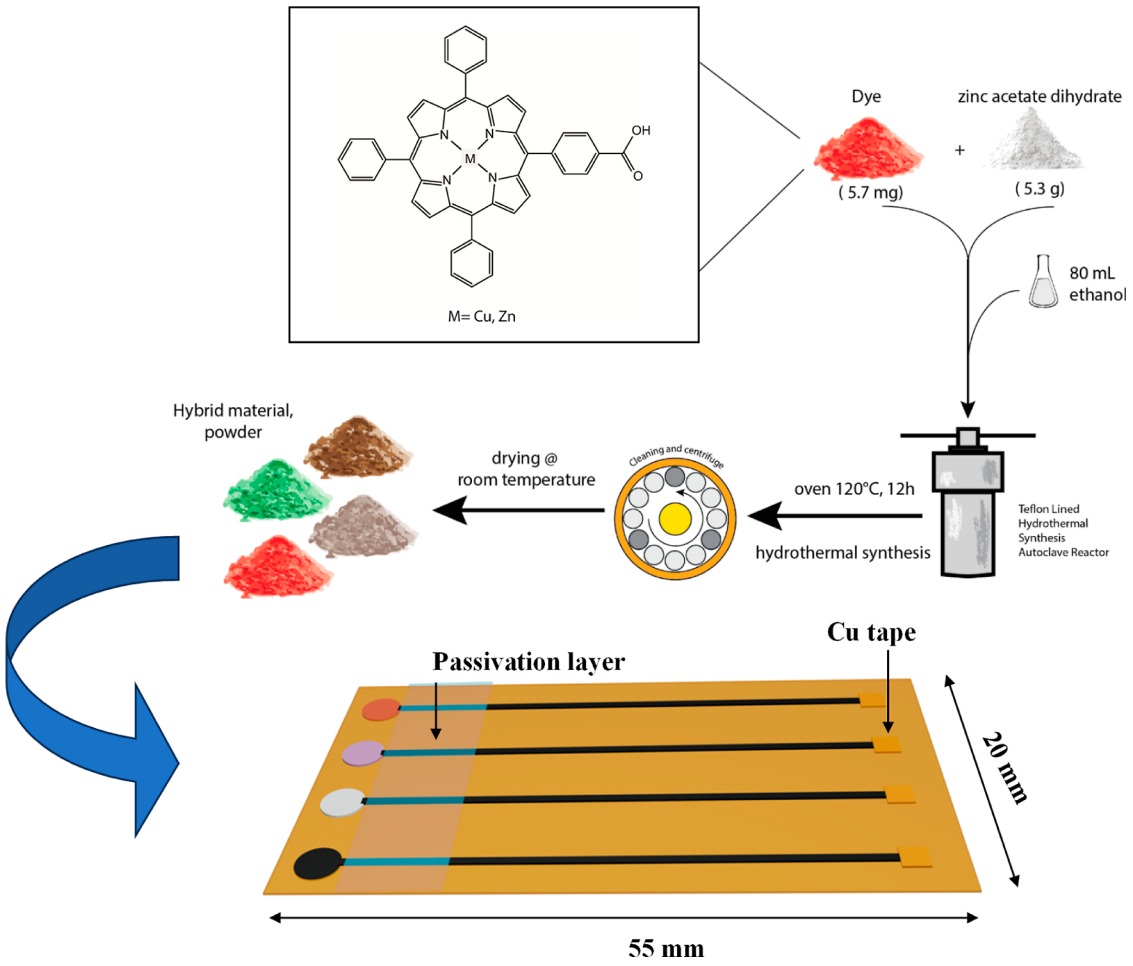

Figure 1. Scheme of the production procedure of functionalized electrodes. Hydrothermal growth of nanoparticles starts from a solution of porphyrins and the ZnO precursor in ethanol. After drying, powders are collected, dissolved in a solvent, and drop-cast onto the LIG electrodes. (Adapted with permission from ref 20 Copyright 2021, American Chemical Society.)

purposes.[11] While LIG electrodes have been predominantly utilized as working electrodes in amperometric arrangements for various applications, their use in potentiometric sensing has been less explored.[12−14]

The inherent sensitivity of LIG electrodes can be further enhanced and diversified by surface functionalization.[15] For example, LIG in combination with a proper ionophore membrane detects ammonia and potassium in urine samples.[16] To investigate this possibility, we chose metalloporphyrins as functional materials due to their remarkable sensitivity in detecting compounds in the atmosphere and solutions.[17] The affinity of porphyrins for ascorbic acid has been previously used in colorimetric and fluorescent sensors.[18,19]

Since previous studies have shown that the sensitivity and selectivity of porphyrins increase when they are arranged at the surface of ZnO nanostructures instead of a compact molecular film, the LIG electrodes were functionalized by a film of porphyrin-capped nanoparticles.[20,21] On the other hand, ZnO itself can contribute to the detection, as suggested by the fact that ZO nanocrystals immobilized on the TiO_2 surface enhance the detection of vitamins in electrochemical sensors.[22]

Potentiometric detection allows the exploitation of a broader range of interaction mechanisms, enabling a thorough exploitation of the interactions between porphyrins and analytes.[23] In potentiometry, the voltage difference between a working electrode and a reference electrode is measured with a potentiostat circuit.[24] This standard approach has been challenged since the seventies by the ion-sensitive field effect transistors (ISFETs), where the gate material is replaced by the electrolytic solution in which the compound of interest is dissolved.[25] ISFETs still require a reference electrode but offer the advantage of transamplification properties of the field effect transistors.

Modern evolutions of the ISFET concept include transistors where the semiconductive channel is made of carbon nanotubes, graphene, or silicon nanowires.[26] These devices require the development of both the transducer (the FET itself) and the sensitive material. EGFETs, a further evolution of ISFETs, use a standard silicon metal-oxide-semiconductor field-effect transistor (MOSFET) to transduce the surface potential of a sensitive electrode connected to the gate terminal, offering advantages in terms of reliability, stability, and conventional electronics interface.[27]

In this paper, we investigate the sensitive properties of EGFETs with electrodes made of LIG, ZnO nanoparticles on LIG, and porphyrin-capped ZnO on LIG. The resulting sensors exhibit high sensitivity and selectivity to ascorbic acid, leveraging the reducing properties of ascorbic acid and the high sensitivity of porphyrins toward electron-donor species. Detection down to the nanomolar range is achieved, surpassing responses to common interferents, such as dopamine, citric acid, and malic acid. This mitigates the cross-selectivity

https://doi.org/10.1021/acsomega.3c09141
ACS Omega 2024, 9, 10650−10659

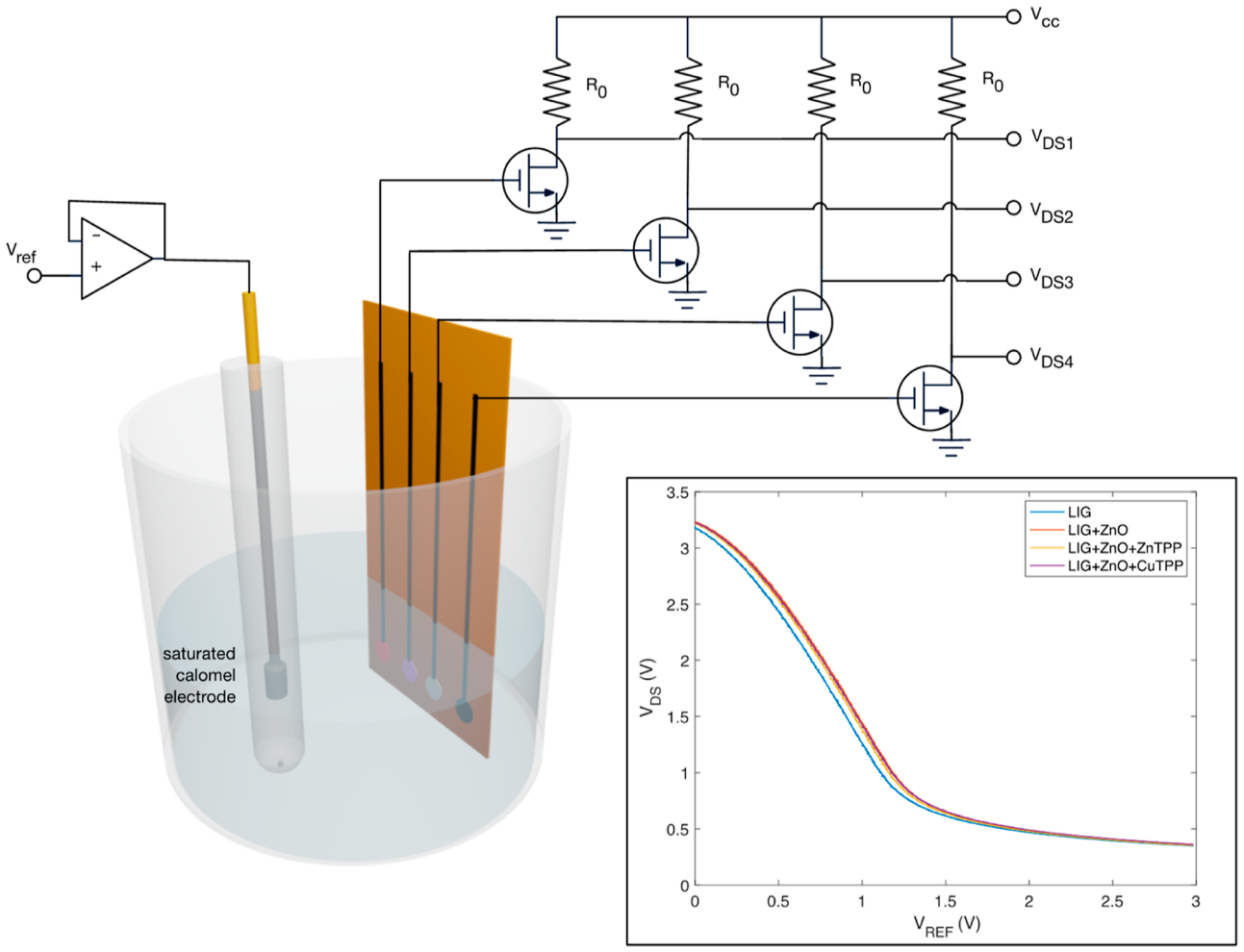

Figure 2. Experimental setup. Each electrode is connected to the gate terminal of a ALD210800A MOSFET. The reference voltage is applied to the saturated calomel reference electrode, and the actual gate voltage is the sum of the potentials of the reference electrode and the sensitive electrode. In the inset, the VTC of the MOSFETs are shown. Since the actual gate voltage is not accessible, the curve is plotted with respect to the reference electrode potential. The effects of the functionalization on LIG electrodes are manifested by the different characteristics of the bare LIG electrode with respect to the others.

observed with LIG electrodes in amperometric setups.[28] The obtained results rival those achieved by enzymatic potentiometric sensors[5] and represent an improvement over previous nonenzymatic ascorbic acid sensors.

MATERIALS AND METHODS

LIG Electrodes. LIG electrodes were created on a 125 μm-thick Kapton sheet by using a Trotec Speedy 100 CO_2 laser cutter (Trotec Laser Inc., Marchtrenk, Austria). LIG was produced with a laser illuminance of 10 W/cm^2, at a rate of 20 cm/s, and with a resolution of 1000 points per inch. Laser engraving was performed in ambient air to achieve a hydrophilic carbonaceous surface suitable for the subsequent deposition of the sensitive material.[11]

The electrodes were fabricated with an active sensing area of approximately 7 mm^2. After laser scribing, the electrodes were cleaned in a solution of water and 2-propanol to remove surface residues and then left to dry at room temperature. A commercial nail polish was applied to passivate the portion of the electrode not in contact with the electrolytic solution.

Functional Sensitive Material. ZnO nanoparticles were synthesized using a hydrothermal method as previously described.[29]

Porphyrin-capped nanoparticles were prepared using a one-pot method in which porphyrins and zinc acetate dihydrate, the ZnO precursor, were mixed, and the material was grown with a hydrothermal procedure.[20] The organic molecules used are 5-(4′-carboxyphenyl)-10,15,20-triphenylporphyrin zinc (referred to as ZnTPP) and 5-(4′-carboxyphenyl)-10,15,20-triphenylporphyrin copper (referred to as CuTPP). These porphyrins have A_3B structures with three equal substituents in the meso position, while the fourth position carries the carboxyl group necessary to bind the molecule to the ZnO surface. The synthesis of free-base porphyrins was carried out through a mixed aldehyde condensation in a 10:1 proportion with 10 equiv of pyrrole in boiling acetic acid. This procedure yields to the A_3B-porphyrin in good yield.[30] Zinc and copper complexes (CuTPP and ZnTPP) were then prepared by following standard metalation protocols used for these macrocycles.[31]

Sensor Preparation. ZnO nanoparticles, whether pure or functionalized, were deposited on LIG by drop-casting from a solution of nanoparticles in *N*-methylpyrrolidone. The sensor array consisted of four sensors: Bare LIG, LIG/ZnO, LIG/ZnO/ZnTPP, and LIG/ZnO/CuTPP.

https://doi.org/10.1021/acsomega.3c09141
ACS Omega 2024, 9, 10650−10659

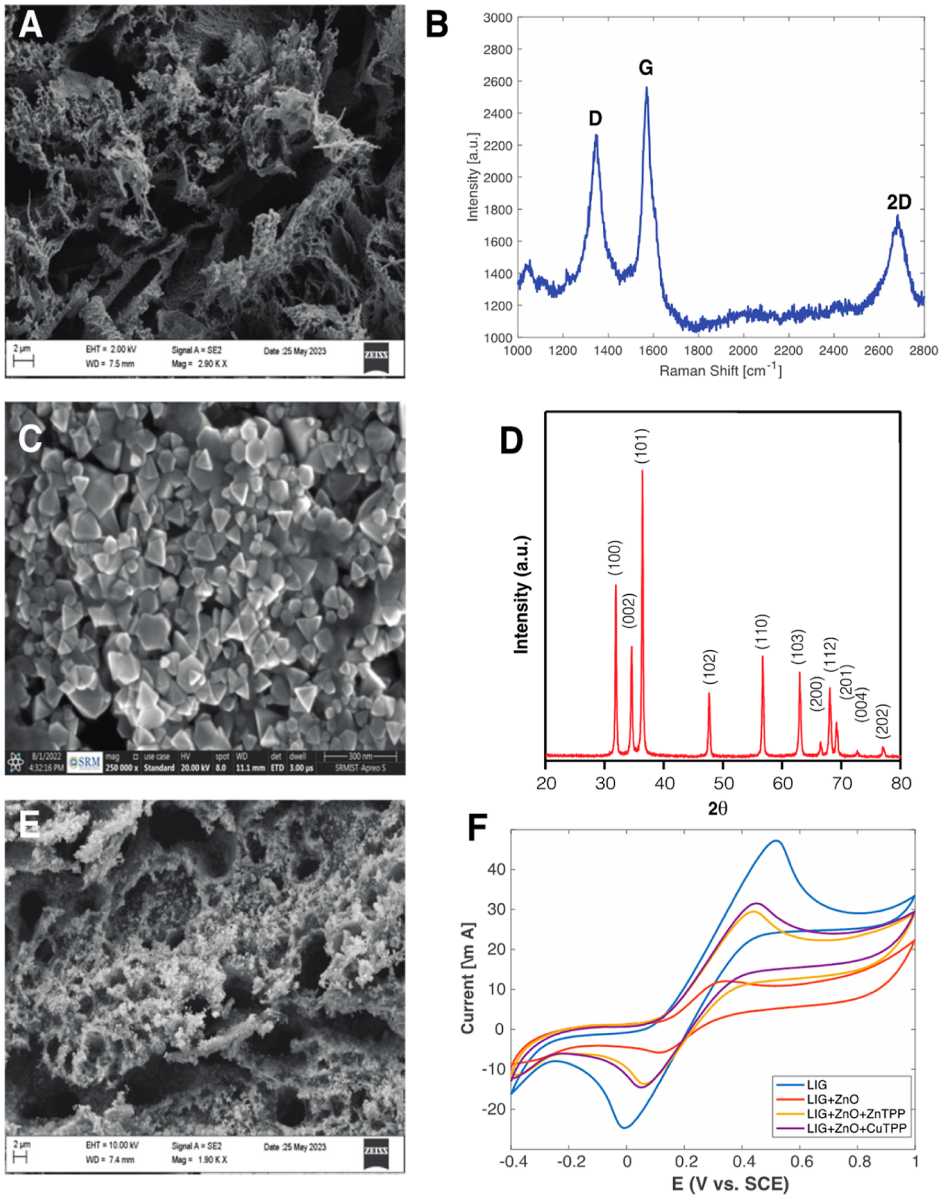

Figure 3. Physical characterization of the sensitive materials. (A) FESEM image of the LIG surface. (B) Raman spectra of LIG powder. (C) FESEM image of ZnO nanoparticles. (D) XRD pattern of ZnO nanoparticles. (E) FESEM image of ZnO-coated LIG. (F) CV measure of 10 mM potassium ferrocyanide in 1× phosphate-buffered saline (1× PBS).

The schematic of the four-electrode preparation is shown in Figure 1.

Morphological, Structural, and Electrochemical Analyses. The crystallinity of ZnO nanoparticles was studied using an X-ray diffractometer (XRD) [Bruker, D8 Advance using Cu Kα nm radiation, λ = 1.5406 nm]. The morphological characterization of electrodes was carried out with a field emission SEM (FESEM) SUPRA 35 instrument (Carl Zeiss SMT, Oberkochen, Germany). Raman spectroscopy was conducted using a Jobin−Yvon−Horiba micro-Raman system (LabRAM ARAMIS) equipped with Ar^+ ion laser (514/488 nm) as excitation source (100 mW).

Cyclic voltammetry (CV) upon potassium ferrocyanide addition was performed by using a PalmSens3 potentiostat/galvanostat. Measurements were carried out at room temperature in a conventional three-electrode system, composed of LIG and functionalized LIG electrodes as the working electrode, a platinum wire as the counter electrode, and a saturated calomel electrode (SCE, 303/SCG/12, AMEL, Italy) as the reference electrode. CV was performed at a scan rate of 10 mV/s.

Sensor Measurement Setup. Figure 2 illustrates a sketch of the sensor arrangement. The EGFETs were obtained connecting each electrode to the gate terminal of a commercial MOSFET device (ALD210800A, Advanced Linear Devices Inc.) with V_{th} = 0 V and transconductance g_m = 1.4 mS. The interface circuit of MOSFETs is designed in order to consider the drain-source voltage (V_{DS}) as the output signal. The same supply voltage (V_{cc} = 3.3 V) and drain resistance (R_0 = 270 Ω) are used for all MOSFETs.

The saturated calomel electrode used for CV was used as a reference electrode. The voltage of the reference electrode was fixed using a 12 bit DAC configurable output amplifier (MAX5352, Analog Devices Inc.). EGFETs have been characterized with the electrode immersed in a buffer solution through the voltage-transfer characteristic (VTC) curve shown

https://doi.org/10.1021/acsomega.3c09141
ACS Omega 2024, 9, 10650−10659

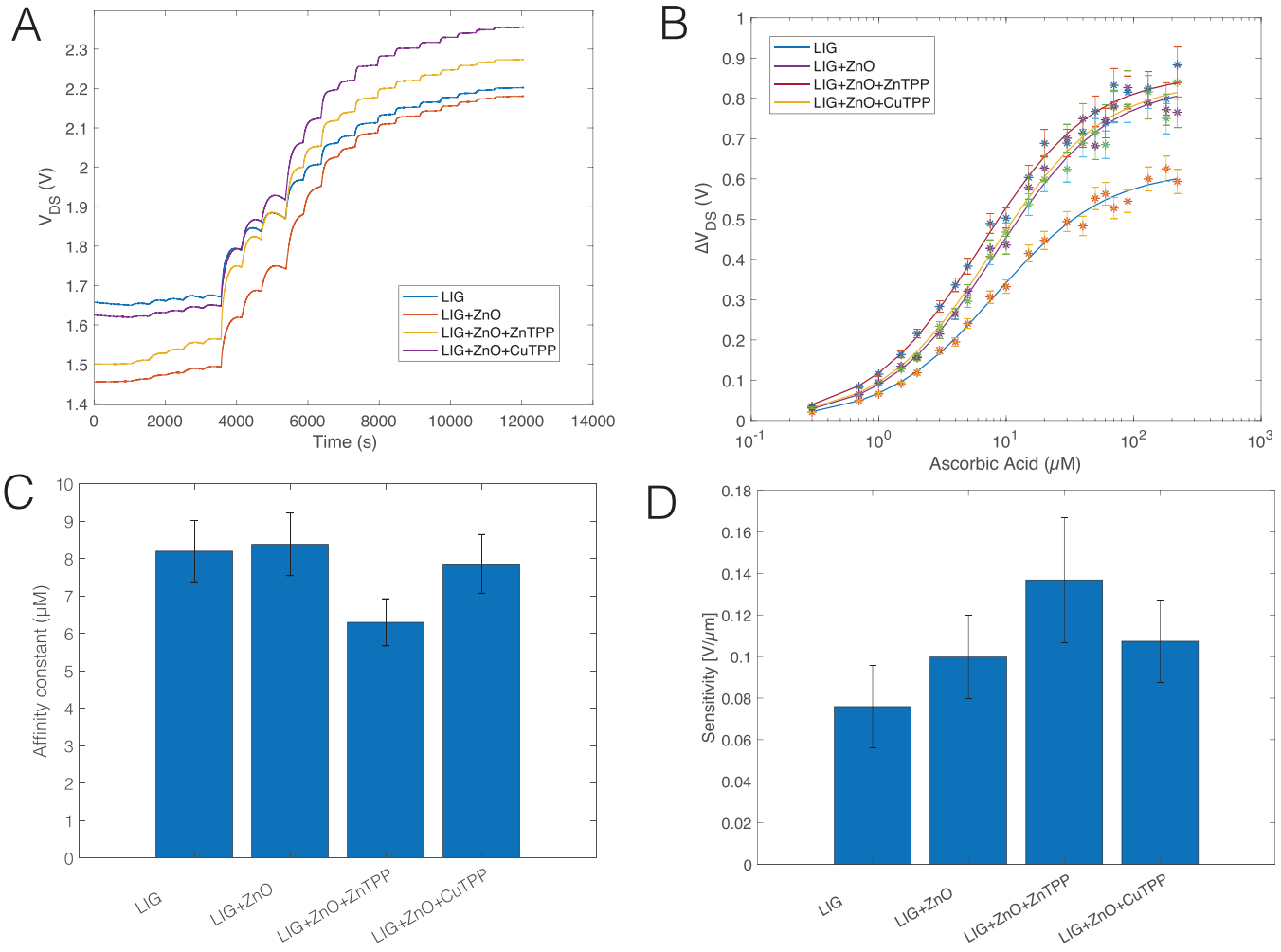

Figure 4. Sensor's response to ascorbic acid. (A) Time progression of sensor's signals at consecutive addition of ascorbic acid in solution. (B) Sensor's response curve obtained calculating the total change of output signal as a function of the concentration. Experimental data are fitted by the Langmuir isotherm function. (C) Affinity constant of the Langmuir isotherm function. (D) Low-concentration sensitivities calculated as the derivative of the fitted Langmuir isotherm function evaluated around the origin.

in the inset of Figure 2. The actual gate voltage is the sum of the reference electrode potential and the electrode potential. The inset of Figure 2 shows the change in surface potential resulting from the functionalization with ZnO and porphyrin-coated ZnO. Measurements were conducted by biasing the transistors in the saturation region while fixing the reference potential at V_{ref} = 0.85 V, as this condition corresponds to the optimal sensitivity of V_{DS} with respect to changes in the gate voltage.[32] To avoid the influence of visible light on porphyrin-coated ZnO, all measurements were performed in dark conditions.

RESULTS AND DISCUSSION

Materials Characterization. Figure 3 depicts the physical characterization of LIG, ZnO nanoparticles, and functionalized LIG. The FESEM image of the LIG electrode (Figure 3A) reveals the typical foam-like structure.[33] The presence of graphene in the electrode is confirmed by Raman spectra (Figure 3B). The first-order *D* peak at 1345 cm^{-1} indicates lattice defects in the sigma bonds, while the first-order *G* peak at 1573 cm^{-1} corresponds to the lattice vibrations of the sp^2 carbon atoms. The second-order 2D peak at 2683 cm^{-1} is related to the graphene structure.[10,34]

ZnO nanoparticles were characterized by FESEM and XRD. The synthesized ZnO nanoparticles exhibited a typical hexagonal structure with an average size of 70 nm (Figure 3C) and high crystallinity (Figure 3D). The XRD pattern was indexed with the JCPDS card no. 36-1451. Figure 3E displays the FESEM image of the ZnO-coated LIG surface; the noticeable differences compared to Figure 3A indicate a complete coverage of the electrode.

The effects of the functionalization on the electrochemical properties of the LIG surface were studied with CV, measuring the redox reaction with potassium ferrocyanide (10 mM in 1× PBS solution). CV curves are shown in Figure 3F. With respect to the bare LIG electrode, the functionalized electrodes show a reduction of the peak current and a shift of the redox potentials. The reduction of current suggests that the functionalization layer increases the resistivity of the electrode, while the changed nature of the electrode surface is demonstrated by the variation in the redox potentials. The current peak of porphyrin-coated LIG is about 3 times larger with respect to the coating with only ZnO nanoparticles.

Chemical Sensitivity and Selectivity. The chemical sensitivity was tested by adding ascorbic acid to an electrolytic solution buffered at pH 7.2 with 1× PBS. To homogenize the

https://doi.org/10.1021/acsomega.3c09141
ACS Omega 2024, 9, 10650−10659

Table 1. Comparison of Performance of Recent Non-enzymatic Sensors of Ascorbic Acid

material	technique	range (μM)	refs
LIG	CV	30−1100	28
poly(furfuryl-alcohol)/graphene oxide	chronoamperometry	50−5000	39
LIG/molecularly imprinted polymer	CV and square wave voltammetry	1000−3500	40
multiwalled carbon nanotube/Ti doped ZnO	CV	100−10,000	41
ZnO nanocrystals on mesoporous TiO_2	differential pulse voltammetry	7−124	22
Zinc oxide/polyaniline nanocomposites	CV	100−1300	42
LSGE/ZnO-porphyrins	EGFET	0.3−220	this work

analyte concentration, the solution was kept stirred by a magnetic bar rotating at 100 rpm.

Figure 4 illustrates the sensor response to ascorbic acid.

Considering the circuit in Figure 2, the relationship between V_{DS} and the electrode potential can be written as

$$V_{DS} = V_{CC} - R_0 I_{DS} = V_{CC} - R_0 g_m (V_{GS} - V_{th})^2 \quad (1)$$

where V_{GS} is the voltage of the gate with respect to the drain, V_{CC} is the MOSFET voltage supply, R_0 is the load resistor, and g_m and V_{th} are the transconductance and the threshold voltage of the MOSFET.

The sequence gate "electrode−electrolyte−reference electrode" can be modeled as a voltage divider circuit where the voltage applied to the reference electrode is portioned between the electrolyte and the sensitive electrode.[35] In the presence of the analyte, each electrode is further charged with an additional potential ($\Delta\phi$) proportional to absorbed molecules. Then, V_{GS} can be written as

$$V_{GS} = \Delta\phi + \frac{V_{ref}}{\frac{R_S}{R_G} + 1} \quad (2)$$

where V_{ref} is the voltage applied to the reference electrode and R_S and R_G are the resistances of the solution and the gate electrode, respectively. Thus, V_{DS} is inversely proportional to the electrode resistance. This relationship is particularly evident in baseline conditions where the sensor with the smallest electrode resistance (the nonfunctionalized LIG) shows the largest V_{DS}.

Figure 4A shows the variation of V_{DS} resulting from the progressive addition of ascorbic acid, ranging from 300 nM up to 220 μM. At each concentration, the sensor response was evaluated as the difference between the steady value of V_{DS} and the baseline value obtained in the absence of ascorbic acid and corresponding to the first 1000 s in Figure 4A. Figure 4B plots the sensor response vs the concentration of ascorbic acid.

The sensor responses are fitted well by the Langmuir isotherm function.

$$\Delta V_{DS} = \Delta V_{max} \frac{C}{K + C} \quad (3)$$

Here, ΔV_{max} is the theoretical saturation value, and K is the affinity constant defined as the concentration at which half of the saturation signal is obtained. The Langmuir isotherm function appropriately fits the experimental data, indicating that the accumulation of ascorbic acid consumes the available adsorbing sites. While the saturation value (ΔV_{max}) may strongly depend on the practical manufacturing of the sensor, constant K in eq 1 is expected to be representative of the interaction between the sensitive material and the analyte. Smaller K values indicate higher affinity of the sensor for the analyte. Affinity constants are compared in Figure 4C. The presence of ZnO and ZnO/CuTPP does not alter the affinity of the sensor, while a clear improvement is obtained, functionalizing the LIG surface with a layer of ZnO/ZnTPP nanoparticles.

The different behavior of sensors with CuTPP and ZnTPP functionalization is a further demonstration of the influence of the metal ion in metalloporphyrins on the sensitivity of sensors. Metals not only affect the coordination, but they also shape the whole environment of the porphyrin changing the intensity of additional sensing mechanisms such as hydrogen bonds, $\pi-\pi$, and van der Waals interactions. Furthermore, the metal affects the mutual interaction of porphyrins and then their molecular arrangement onto the ZnO surface.[23] Previous investigations about gas sensing properties have shown that ZnO/ZnTPP outperforms ZnO/CuTPP in terms of sensitivity and selectivity with respect to amines and aromatic compounds.[36]

A useful quantification of the performance of the sensors can be obtained by calculating the sensitivity which is defined as the derivative of the sensor response with respect to the concentration of the analyte.[37] Since the response curve is not linear, the sensitivity is a function of the concentration and is maximum at the origin, decreasing as the concentration increases. A convenient figure of the sensitivity is achieved at a low concentration where it is

$$S_{c\to 0} = \lim_{c\to 0} \frac{d\Delta V_{DS}}{dC} = \frac{\Delta V_{max}}{K} \quad (4)$$

Figure 4D compares the low-concentration sensitivity of the four sensors calculated in five sensors obtained from the same batch production. Although all sensors exhibit good sensitivity with respect to ascorbic acid, those coated with ZnO and porphyrins demonstrate the highest sensitivity. The sensor with the highest affinity (LIG + ZnO + ZnTPP) is also the most sensitive. The other sensors, even with similar affinity constants, exhibit different sensitivities.

Lack of correlation between the Langmuir affinity constant and the low-concentration sensitivity can be observed when sensors of different morphologies are compared. For instance, it is found in heterojunctions of phthalocyanines with polymers of corroles growth with different thicknesses and the morphologies.[38]

Sensitivity plays a crucial role in determining the limit of detection (LOD). The LOD has been calculated using the following relationship[37]

$$LOD = \frac{\sigma_{VDS}}{S_{c=0}} \quad (5)$$

where σ_{Vds} is the standard deviation of the sensor signal and $S_{c=0}$ is the sensitivity at the origin. The standard deviation has been calculated on the signal before the injection of the smallest concentration of ascorbic acid; this corresponds to the

https://doi.org/10.1021/acsomega.3c09141
ACS Omega 2024, 9, 10650−10659

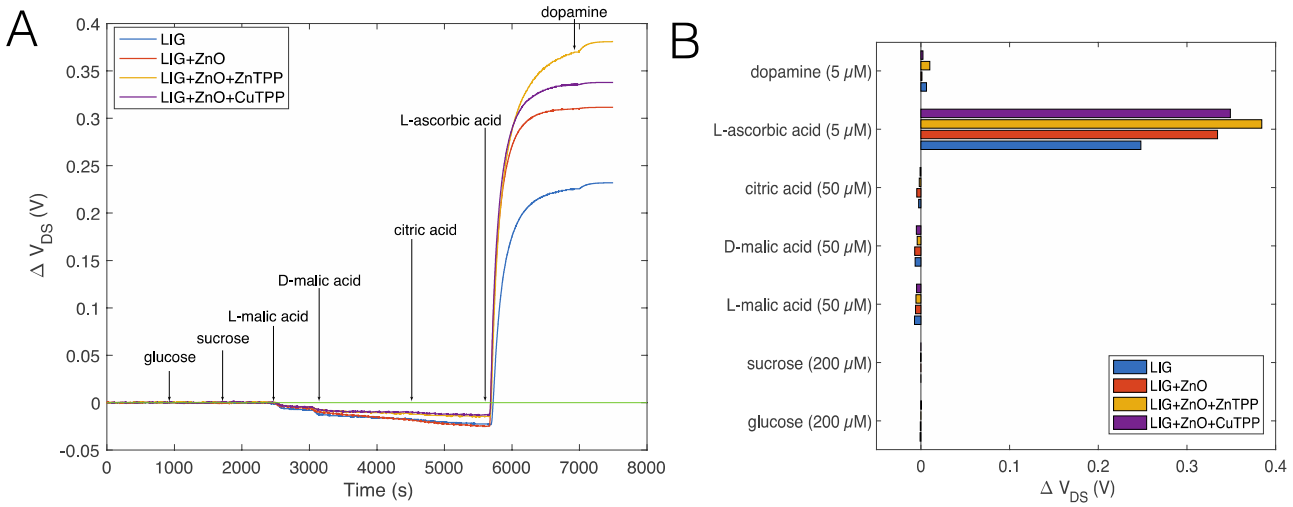

Figure 5. Selectivity tests. (A) Sensors' signal in consecutive addition of interferents. (B) Net response of the sensors to ascorbic acid and interferents.

first 1000 s in Figure 4A. The average standard deviations of the signals in a cohort of five replicated sensors are estimated in the range from 0.4 mV for the LIG + ZnO + ZnTPP sensor to 31.3 mV for the LIG-based sensor. Thus, considering the low-concentration sensitivity shown in Figure 4C, the sensor's LODs range from 3 ± 0.7 nM for LIG + ZnO + ZnTPP to 31 ± 2 nM for LIG. In Table 1, the results are compared with the literature results achieved by diverse electrochemical sensors.

The sensitivity of LIG to ascorbic acid is not surprising because it is known that the density of electronic states at the edge sites of LIG enhances the electron-transfer kinetics compared to other carbon materials.[12] Furthermore, since porphyrins are well-known electrocatalysts, their presence on the sensor surface likely improves its basic performance.

To study the selectivity, the sensors were exposed to a sequence of possible interferent compounds, including sugars (glucose and fructose), organic acids (L-malic acid, D-malic acid, and citric acid), and dopamine.

Glucose and sucrose are simple carbohydrates commonly found in physiological systems. On the other hand, dopamine is associated with ascorbic acid, so that they can interfere with each other. These two compounds can be simultaneously identified in amperometric sensors exploiting the different oxidation potential on the same inorganic surfaces, such as metal oxides and graphene.[43,44]

Selectivity tests were performed at different analyte concentrations. Glucose and sucrose were tested at 200 μM, L-malic acid, D-malic acid, and citric acid at 50 μM and ascorbic acid and dopamine at 5 μM.

The results of the selectivity tests are reported in Figure 5. Figure 5A displays the signals of sensors during the consecutive addition of analytes, while Figure 5B compares the responses of sensors to each analyte. The response to ascorbic acid dominates over the interferents. The ratio of signals to ascorbic acid compared to dopamine ranges from 38, for LIG and ZnO-coated LIG, up to 150 and 270 for sensors coated with CuTPP and ZnTPP, respectively. The ratio of signals is even larger compared to dopamine even considering that citric and malic acid are tested at a concentration of 50 μM, 1 order of magnitude higher than ascorbic acid. Finally, the response to sucrose and glucose is barely detectable.

Notably, the response of sensors to malic and citric acids is negative compared to ascorbic acid. Citric acid and malic acid are triprotic and diprotic species, respectively; in the buffered conditions, they are present as citrate and malate ions, and consequently, they give a small anionic, negative potentiometric response. Ascorbic acid is a weaker acid, and in the solution conditions, the interaction mechanisms with the sensor surface should probably follow different pathways, inducing the high positive response, which has the same positive character of the small response to dopamine, which is positively charged in the solution conditions. As an additional argument, the binding of ascorbic acid is particularly strong, and the sensors, even when exposed back to the PBS solution, do not recover back to the initial conditions (data not shown). The sensors maintain their dynamic response, but as the concentration of absorbed ascorbic acid increases, the sensor surface tends to be permanently saturated. The noncomplete reversibility of the sensor signal suggests that in the case of ascorbic acid, more efficient and peculiar interactions take place.

Tests on Real Samples. Finally, the detection of ascorbic acid in real samples was tested. For this purpose, a commercial food supplement of L-arginine was considered (Bioarginina, Damor Farmaceutica, Napoli, Italia). L-arginine is an amino acid expected to have beneficial effects on several physiological processes.[45]

The tested product contained 8.3 g per 100 mL of L-arginine. A vitamin C-enriched version of Bioarginina is also available (Bioarginina C, Damor Farmaceutica, Napoli, Italia). Sucrose and citric acid are the major excipients in both products, and as mentioned earlier, the sensitivity of the sensors to these compounds is negligible. The products are liquid and contain the same amount of L-arginine, while 2500 mg per 100 mL of ascorbic acid is added to the buffered solution. The products were purchased from a local pharmacy and stored at room temperature.

Both products were measured by adding a drop to 10 mL of 1× PBS at pH 7.2. From the composition declared by the producer, the added products correspond in one case to 23.8 μM L-arginine and, in the other case, to 23.8 μM L-arginine and 7 μM ascorbic acid.

https://doi.org/10.1021/acsomega.3c09141
ACS Omega 2024, 9, 10650−10659

Figure 6 displays the response of the four sensors to the basic formulation and to the product added with ascorbic acid.

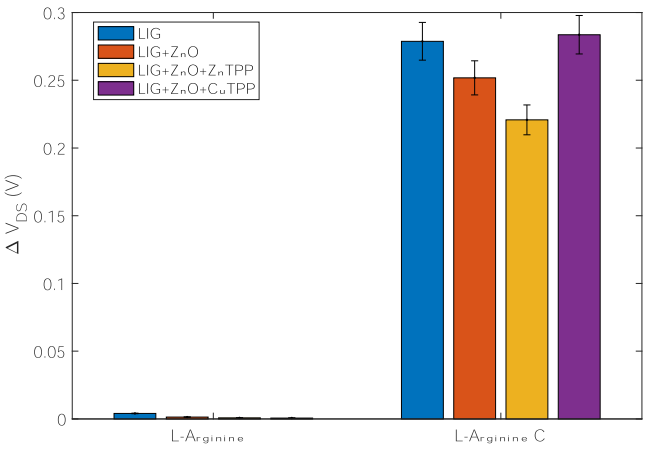

Figure 6. Response of sensors to L-arginine and L-arginine added with the C vitamin.

None of the sensors is sensitive to the basic formulation, but they show a substantial signal when exposed to the L-arginine plus vitamin C.

CONCLUSIONS

In this paper, we have successfully demonstrated the nonenzymatic detection of ascorbic acid using a LIG electrode configured as an EGFET. The LIG electrode exhibits remarkable sensitivity and selectivity to ascorbic acid with an estimate LOD on the order of 31 nM. The sensor's performance is significantly enhanced by coating the LIG with ZnO nanoparticles and porphyrin-capped ZnO nanoparticles. The sensor functionalized with ZnTPP-coated ZnO achieved a LOD of 3 nM. The combinations of these materials demonstrate excellent selectivity, especially in the presence of common interferents like dopamine. The interaction with ascorbic acid follows different pathways with respect to the interaction with other organic acids. A deeper investigation of the nature of the interaction will help to optimize the sensor and elucidate the sensing properties of LIG and functionalized LIG.

The signal to 5 μM ascorbic acid compared to the same concentration of dopamine is 38 times larger in LIG and LIG−ZnO. However, the porphyrin-functionalized electrodes exhibit even more large response ratios, with values of 153 and 278 for CuTPP and ZnTPP, respectively. Thus, the functionalization with porphyrins not only enhances sensitivity but also greatly improves selectivity.

Furthermore, we have also demonstrated the detection of ascorbic acid by measuring the response to a commercial food supplement containing L-arginine and vitamin C-enriched L-arginine.

Ultimately, this article provides further evidence of the exceptional sensing properties of LIG-based sensors. In this case, the binding of analytes has been transduced using an EGFET configuration with a standard commercial MOSFET. The combination of LIG electrodes on polyimide surfaces with widely available electronic devices offers the potential to develop low-cost, reliable, and stable sensors for a wide range of applications.

AUTHOR INFORMATION

Corresponding Author

Corrado Di Natale − *Department of Electronic Engineering, University of Rome Tor Vergata, 00133 Rome, Italy;* orcid.org/0000-0002-0543-4348; Email: dinatale@uniroma2.it

Authors

Kishore Pushparaj − *Department of Electronic Engineering, University of Rome Tor Vergata, 00133 Rome, Italy;* orcid.org/0000-0002-6170-7291

Alexandro Catini − *Department of Electronic Engineering, University of Rome Tor Vergata, 00133 Rome, Italy*

Rosamaria Capuano − *Department of Electronic Engineering, University of Rome Tor Vergata, 00133 Rome, Italy*

Valerio Allegra − *Department of Electronic Engineering, University of Rome Tor Vergata, 00133 Rome, Italy*

Gabriele Magna − *Department of Chemical Science and Technologies, University of Rome Tor Vergata, 00133 Rome, Italy;* orcid.org/0000-0003-2140-0110

Gianni Antonelli − *Department of Electronic Engineering, University of Rome Tor Vergata, 00133 Rome, Italy;* orcid.org/0000-0002-4658-4000

Eugenio Martinelli − *Department of Electronic Engineering, University of Rome Tor Vergata, 00133 Rome, Italy*

Antonio Agresti − *Department of Electronic Engineering, University of Rome Tor Vergata, 00133 Rome, Italy;* orcid.org/0000-0001-6581-0387

Sara Pescetelli − *Department of Electronic Engineering, University of Rome Tor Vergata, 00133 Rome, Italy;* orcid.org/0000-0002-3336-2425

Yuvaraj Sivalingam − *Department of Physics and Nanotechnology, SRM Institute of Science and Technology, Kattankulathur 603203 Tamil Nadu, India;* orcid.org/0000-0002-2079-1570

Roberto Paolesse − *Department of Chemical Science and Technologies, University of Rome Tor Vergata, 00133 Rome, Italy;* orcid.org/0000-0002-2380-1404

Complete contact information is available at: https://pubs.acs.org/10.1021/acsomega.3c09141

Notes

The authors declare no competing financial interest.

ACKNOWLEDGMENTS

The financial support of Project ECS 0000024 Rome Technopole,—CUP B83C22002820006, NRP Mission 4 Component 2 Investment 1.5, funded by the European Union—NextGenerationEU", is gratefully acknowledged.

REFERENCES

(1) Njus, D.; Kelley, P. M.; Tu, Y.-J.; Schlegel, H. B. Ascorbic Acid: The Chemistry Underlying Its Antioxidant Properties. *Free Radical Biol. Med.* **2020**, *159*, 37−43.

(2) Pisoschi, A. M.; Pop, A.; Serban, A. I.; Fafaneata, C. Electrochemical Methods for Ascorbic Acid Determination. *Electrochim. Acta* **2014**, *121*, 443−460.

(3) Malik, M.; Narwal, V.; Pundir, C. S. Ascorbic Acid Biosensing Methods: A Review. *Process Biochem.* **2022**, *118*, 11−23.

(4) Huang, L.; Tian, S.; Zhao, W.; Liu, K.; Guo, J. Electrochemical Vitamin Sensors: A Critical Review. *Talanta* **2021**, *222*, 121645.

(5) Kuo, P.-Y.; Lai, W.-H.; Huang, M.-J.; Chang, C.-H.; Wang, T.-H. The Sensing Characteristics Investigation of a Potentiometric

https://doi.org/10.1021/acsomega.3c09141
ACS Omega 2024, 9, 10650−10659

Ascorbic Acid Biosensor Integrated with Analog-to-Digital Converter. *IEEE Trans. Nanotechnol.* **2023**, *22*, 36−44.
(6) Wei, M.; Qiao, Y.; Zhao, H.; Liang, J.; Li, T.; Luo, Y.; Lu, S.; Shi, X.; Lu, W.; Sun, X. Electrochemical Non-Enzymatic Glucose Sensors: Recent Progress and Perspectives. *Chem. Commun.* **2020**, *56* (93), 14553−14569.
(7) Shen, L.; Liang, Z.; Chen, Z.; Wu, C.; Hu, X.; Zhang, J.; Jiang, Q.; Wang, Y. Reusable Electrochemical Non-Enzymatic Glucose Sensors Based on Au-Inlaid Nanocages. *Nano Res.* **2022**, *15* (7), 6490−6499.
(8) Qiao, Y.; Liu, Q.; Lu, S.; Chen, G.; Gao, S.; Lu, W.; Sun, X. High-Performance Non-Enzymatic Glucose Detection: Using a Conductive Ni-MOF as an Electrocatalyst. *J. Mater. Chem. B* **2020**, *8* (25), 5411−5415.
(9) Chen, T.; Liu, D.; Lu, W.; Wang, K.; Du, G.; Asiri, A. M.; Sun, X. Three-Dimensional Ni2P Nanoarray: An Efficient Catalyst Electrode for Sensitive and Selective Nonenzymatic Glucose Sensing with High Specificity. *Anal. Chem.* **2016**, *88* (16), 7885−7889.
(10) Lin, J.; Peng, Z.; Liu, Y.; Ruiz-Zepeda, F.; Ye, R.; Samuel, E. L. G.; Yacaman, M. J.; Yakobson, B. I.; Tour, J. M. Laser-Induced Porous Graphene Films from Commercial Polymers. *Nat. Commun.* **2014**, *5*, 5714.
(11) Ye, R.; James, D. K.; Tour, J. M. Laser-Induced Graphene: From Discovery to Translation. *Adv. Mater.* **2019**, *31*, 1803621.
(12) Wan, Z.; Nguyen, N.-T.; Gao, Y.; Li, Q. Laser Induced Graphene for Biosensors. *Sustainable Mater. Technol.* **2020**, *25*, No. e00205.
(13) Liu, J.; Ji, H.; Lv, X.; Zeng, C.; Li, H.; Li, F.; Qu, B.; Cui, F.; Zhou, Q. Laser-Induced Graphene (LIG)-Driven Medical Sensors for Health Monitoring and Diseases Diagnosis. *Microchim. Acta* **2022**, *189*, 54.
(14) Wanjari, V. P.; Duttagupta, S. P.; Singh, S. P. Dual Linear Range Laser-Induced Graphene-Based Sensor for 4-Nitrophenol Detection in Water. *ACS Appl. Nano Mater.* **2023**, *6* (13), 11351−11360.
(15) Vivaldi, F. M.; Dallinger, A.; Bonini, A.; Poma, N.; Sembranti, L.; Biagini, D.; Salvo, P.; Greco, F.; Di Francesco, F. Three-Dimensional (3D) Laser-Induced Graphene: Structure, Properties, and Application to Chemical Sensing. *ACS Appl. Mater. Interfaces* **2021**, *13*, 30245−30260.
(16) Kucherenko, I. S.; Sanborn, D.; Chen, B.; Garland, N.; Serhan, M.; Forzani, E.; Gomes, C.; Claussen, J. C. Ion-Selective Sensors Based on Laser-Induced Graphene for Evaluating Human Hydration Levels Using Urine Samples. *Adv. Mater. Technol.* **2020**, *5* (6), 1901037.
(17) Paolesse, R.; Nardis, S.; Monti, D.; Stefanelli, M.; Di Natale, C. Porphyrinoids for Chemical Sensor Applications. *Chem. Rev.* **2017**, *117* (4), 2517−2583.
(18) Sebarchievici, I.; Lascu, A.; Fagadar-Cosma, G.; Palade, A.; Fringu, I.; Birdeanu, M.; Taranu, B.; Fagadar-Cosma, E. Optical and Electrochemical-Mediated Detection of Ascorbic Acid Using Manganese Porphyrin and Its Gold Hybrids. *C. R. Chim.* **2018**, *21* (3−4), 327−338.
(19) Li, M.; Zhang, S.; Li, H.; Chen, M. Cerium/Polyacrylic Acid Modified Porphyrin Metal-Organic Framework as Fluorescence and Photothermal Sensor for Ascorbic Acid Measurement. *Talanta* **2023**, *252*, 123825.
(20) Magna, G.; Muduganti, M.; Stefanelli, M.; Sivalingam, Y.; Zurlo, F.; Di Bartolomeo, E.; Catini, A.; Martinelli, E.; Paolesse, R.; Di Natale, C. Light-Activated Porphyrinoid-Capped Nanoparticles for Gas Sensing. *ACS Appl. Nano Mater.* **2021**, *4* (1), 414−424.
(21) Magna, G.; Dinc Zor, S.; Catini, A.; Capuano, R.; Basoli, F.; Martinelli, E.; Paolesse, R.; Di Natale, C. Surface Arrangement Dependent Selectivity of Porphyrins Gas Sensors. *Sens. Actuators, B* **2017**, *251*, 524−532.
(22) Manoj, D.; Rajendran, S.; Gracia, F.; Naushad, M.; Santhamoorthy, M.; Soto-Moscoso, M.; Gracia-Pinilla, M. A. Engineering ZnO Nanocrystals Anchored on Mesoporous TiO_2 for Simultaneous Detection of Vitamins. *Biochem. Eng. J.* **2022**, *186*, 108585.
(23) Di Natale, C.; Monti, D.; Paolesse, R. Chemical Sensitivity of Porphyrin Assemblies. *Mater. Today* **2010**, *13* (7−8), 46−52.
(24) Bakker, E.; Pretsch, E. Modern Potentiometry. *Angew. Chem., Int. Ed.* **2007**, *46*, 5660−5668.
(25) Bergveld, P. Development of an Ion-Sensitive Solid-State Device for Neurophysiological Measurements. *IEEE Trans. Biomed. Eng.* **1970**, *BME-17* (1), 70−71.
(26) Moser, N.; Lande, T. S.; Toumazou, C.; Georgiou, P. ISFETs in CMOS and Emergent Trends in Instrumentation: A Review. *IEEE Sens. J.* **2016**, *16*, 6496−6514.
(27) Pullano, S. A.; Critello, C. D.; Mahbub, I.; Tasneem, N. T.; Shamsir, S.; Islam, S. K.; Greco, M.; Fiorillo, A. S. EGFET-Based Sensors for Bioanalytical Applications: A Review. *Sensors (Switzerland)* **2018**, *18*, 4042.
(28) Nayak, P.; Kurra, N.; Xia, C.; Alshareef, H. N. Highly Efficient Laser Scribed Graphene Electrodes for On-Chip Electrochemical Sensing Applications. *Adv. Electron. Mater.* **2016**, *2* (10), 1600185.
(29) Aneesh, P. M.; Vanaja, K. A.; Jayaraj, M. K. Synthesis of ZnO Nanoparticles by Hydrothermal Method. In *Proc. SPIE 6639, Nanophotonic Materials IV*; SPIE, 2007; Vol. *6639*..
(30) Stefanelli, M.; Monti, D.; Van Axel Castelli, V.; Ercolani, G.; Venanzi, M.; Pomarico, G.; Paolesse, R. Chiral Supramolecular Capsule by Ligand Promoted Self-Assembly of Resorcinarene-Zn Porphyrin Conjugate. *J. Porphyrins Phthalocyanines* **2008**, *12* (12), 1279−1288.
(31) Sanders, J. K. M.; Bampos, N.; Clyde-Watson, Z.; Darling, S. L.; Hawley, J. C.; Kim, H.-J.; Mak, C. C.; Webb, S. J. Axial Coordination Chemistry of Metalloporphyrins. *ChemInform* **2003**, *34*, 1−48.
(32) Rao, L.; Wang, P.; Qian, Y.; Zhou, G.; Nötzel, R. Comparison of the Extended Gate Field-Effect Transistor with Direct Potentiometric Sensing for Super-Nernstian InN/InGaN Quantum Dots. *ACS Omega* **2020**, *5* (50), 32800−32805.
(33) Chen, X.; Li, R.; Niu, G.; Xin, M.; Xu, G.; Cheng, H.; Yang, L. Porous Graphene Foam Composite-Based Dual-Mode Sensors for Underwater Temperature and Subtle Motion Detection. *Chem. Eng. J.* **2022**, *444*, 136631.
(34) Ferrari, A. C.; Meyer, J. C.; Scardaci, V.; Casiraghi, C.; Lazzeri, M.; Mauri, F.; Piscanec, S.; Jiang, D.; Novoselov, K. S.; Roth, S.; Geim, A. K. Raman Spectrum of Graphene and Graphene Layers. *Phys. Rev. Lett.* **2006**, *97* (18), 187401.
(35) Könemund, L.; Neumann, L.; Hirschberg, F.; Biedendieck, R.; Jahn, D.; Johannes, H.-H.; Kowalsky, W. Functionalization of an Extended-Gate Field-Effect Transistor (EGFET) for Bacteria Detection. *Sci. Rep.* **2022**, *12* (1), 4397.
(36) Magna, G.; Catini, A.; Kumar, R.; Palmacci, M.; Martinelli, E.; Paolesse, R.; di Natale, C. Conductive Photo-Activated Porphyrin-ZnO Nanostructured Gas Sensor Array. *Sensors (Switzerland)* **2017**, *17* (4), 747.
(37) D'Amico, A.; Di Natale, C. A Contribution on Some Basic Definitions of Sensors Properties. *IEEE Sens. J.* **2001**, *1* (3), 183−190.
(38) Di Zazzo, L.; Kumar, A.; Meunier-Prest, R.; Di Natale, C.; Paolesse, R.; Bouvet, M. Electrosynthesized Copper Polycorroles as Versatile Materials in Double Lateral Heterojunctions. *Chem. Eng. J.* **2023**, *458*, 141465.
(39) Fernandes Loguercio, L.; Thesing, A.; da Silveira Noremberg, B.; Vasconcellos Lopes, B.; Kurz Maron, G.; Machado, G.; Pope, M. A.; Lenin Villarreal Carreno, N. Direct Laser Writing of Poly(Furfuryl Alcohol)/Graphene Oxide Electrodes for Electrochemical Determination of Ascorbic Acid. *ChemElectroChem* **2022**, *9* (17), No. e202200334.
(40) Marques, A. C.; Cardoso, A. R.; Martins, R.; Sales, M. G. F.; Fortunato, E. Laser-Induced Graphene-Based Platforms for Dual Biorecognition of Molecules. *ACS Appl. Nano Mater.* **2020**, *3* (3), 2795−2803.
(41) Pitiphattharabun, S.; Meesombad, K.; Panomsuwan, G.; Jongprateep, O. MWCNT/Ti-Doped ZnO Nanocomposite as

https://doi.org/10.1021/acsomega.3c09141
ACS Omega 2024, 9, 10650−10659

Electrochemical Sensor for Detecting Glutamate and Ascorbic Acid. *Int. J. Appl. Ceram. Technol.* **2022**, *19* (1), 467−479.
(42) Kadri, Y.; Bekri-Abbess, I.; Herrasti, P. Highly Sensitive Enzyme-Free Sensor Based on a Carbon Paste Electrode Modified with Binary Zinc Oxide/Polyaniline Nanocomposites for Dopamine, Ascorbic Acid and Uric Acid Sensing. *Electroanalysis* **2023**, *35* (4), No. e202200248.
(43) Coroş, M.; Pruneanu, S.; Stefan-van Staden, R.-I. Review—Recent Progress in the Graphene-Based Electrochemical Sensors and Biosensors. *J. Electrochem. Soc.* **2020**, *167* (3), 037528.
(44) Liu, X.; Liu, J. Biosensors and Sensors for Dopamine Detection. *View* **2021**, *2*, 20200102.
(45) Szlas, A.; Kurek, J. M.; Krejpcio, Z. The Potential of L-Arginine in Prevention and Treatment of Disturbed Carbohydrate and Lipid Metabolism—A Review. *Nutrients* **2022**, *14*, 961.

https://doi.org/10.1021/acsomega.3c09141
ACS Omega 2024, 9, 10650−10659